Hierarchical Nanowires Synthesized by Supramolecular Stepwise Polymerization

Zeliang Zhuang, Tao Jiang, Jiaping Lin,* Liang Gao, Chaoying Yang, Liquan Wang,* and Chunhua Cai

Abstract: *The self-organization of pre-assembled aggregates is an efficient stepwise strategy for fabricating nanostructures with a second level of hierarchy. Herein, we report that anisotropic spindle-like micelles, self-assembled from poly-peptide graft copolymers with rigid backbones, can serve as ideal pre-assembled subunits for constructing one-dimensional materials with hierarchical structures. By adding organic solvents and dialyzing against water, reactive points can be generated at the ends of the spindle-like micelles, which subsequently drive the anisotropic micelles to grow as rods in a chain and eventually self-assemble into hierarchical nano-wires in a stepwise manner. The second self-assembly step is a hierarchical process that resembles step polymerization. Hierarchical structures can be precisely synthesized by this new type of polymerization. These nanostructures can be tailored by the activity of the reactive points, which depends on the nature of the solvent and the molecular architecture.*

Natural materials, which possess fascinating hierarchical structures, are typically created from hierarchical self-assem-bly processes.[1] For example, *Streptobacillus*, a genus of anaerobic bacteria, exhibit hierarchical structures in which a series of small rod-like bacilli are distributed along a long chain.[2] The chain-like structures are formed by hierarchical self-assembly—growing in culture as rods in chains. This natural phenomenon has inspired various bottom-up strat-egies, such as stepwise self-assembly, to design and fabricate intricate materials, particularly one-dimensional materials.[3]

In the stepwise self-assembly of soft matter, such as copolymers, the first step involves the molecular-level assem-bly of amphiphilic copolymers into diverse aggregates, such as micelles and vesicles,[4] whereas the second step involves further assembly of the aggregates into structures that have a second level of hierarchy. The second assembly step can be induced by temperature changes, electrostatic attraction, crystallization, and solvent selectivity.[3a,e,f,5,6] Such a process is analogous to polymerization in synthetic polymers but

occurs at considerably larger length scales, similar to that observed in nanoparticle and *Streptobacillus* systems.[2,7] For example, Pochan et al. prepared spherical micelles of poly(acrylic acid)-*block*-poly(methyl acrylate)-*block*-poly-styrene in solution.[8] After introducing tetrahydrofuran (THF) into the solution in the presence of diamines, the micelles underwent a sphere-to-disk morphological transi-tion, which allowed for preferential growth of the micelles in one dimension to form cylindrical nanostructures with alter-nating lamellae. The success in creating such nanostructures by polymerizing pre-assemblies can be attributed to a directed stepwise self-assembly process that is facilitated by the anisotropy of the disk-like pre-assemblies and long-range electrostatic interactions between charged blocks with multi-valent counterions. Although reports are available on the stepwise self-assembly process,[9] understanding the under-lying principles still presents a challenge because of the complexity of these processes.

Herein, we demonstrate a stepwise self-assembly method-ology for achieving one-dimensional growth of anisotropic pre-assemblies. Our previous studies revealed that poly-peptide-based graft copolymers bearing rigid α-helix blocks are able to self-assemble into distinct aggregates with unique structures, for example, anisotropic spindle-like micelles.[10] In this study, it was discovered that these spindle-like micelles can act as pre-assemblies that further self-assemble into nanowires. We begin by considering the active spindle-like micelles that are formed by poly(γ-benzyl-ʟ-glutamate)-*graft*-poly(ethylene glycol) (PBLG-*g*-PEG) graft copolymers in THF/dimethylformamide (DMF)/water mixed solvents. The weight average molecular weights of the PBLG backbone and the PEG grafted chains were 170000 and 750 g mol^{-1}, respectively, and the grafting degree of the PEG was 1.23%. In the first step, spindle-like subunits were typically prepared by adding selective solvents (water, 2.5 mL) to PBLG-*g*-PEG/THF/DMF (10 mL of solution with a polymer concentration of 0.67 g L^{-1}). The volume ratio of THF/DMF in the initial solution is 1/1, from which well-structured spindles can be obtained. Experimental details are provided in Section 1 of the Supporting Information. In the second step, 10 mL of DMF was pipetted into the initial subunit solution to create reactive points at each end of the spindle-like subunits, and then the solution was dialyzed against water. As a result of the imperfect coverage of PEG chains at both ends of the spindle, higher energy can be generated, which endows the reactive points at the ends with sufficient activity to induce further self-assembly of the subunits.

A TEM image of the pre-assembled subunits revealed uniform spindle-like micelles with a mean length of approx-

[*] Dr. Z. Zhuang, Dr. T. Jiang, Prof. Dr. J. Lin, Dr. L. Gao, Dr. C. Yang, Dr. L. Wang, Dr. C. Cai
Shanghai Key Laboratory of Advanced Polymeric Materials, State Key Laboratory of Bioreactor Engineering, Key Laboratory for Ultrafine Materials of Ministry of Education, School of Materials Science and Engineering, East China University of Science and Technology
Shanghai 200237 (China)
E-mail: jlin@ecust.edu.cn
lq_wang@ecust.edu.cn
Homepage: http://jlinlab.ecust.edu.cn/

imately 400 nm (Figure 1 a). In the second self-assembly step, nanowire structures with connected subunits were formed (Figure 1 b). The connectedness of the subunits was also confirmed using cryo-TEM (Figure 1 c). Because cryo-TEM revealed the same morphology as conventional TEM, the possibility that drying effects could have contributed to the formation of the observed connected structure can be ruled out. The nanowire structures were further examined using SEM (Figure 1 d) and AFM (Figure 1 e). The AFM image
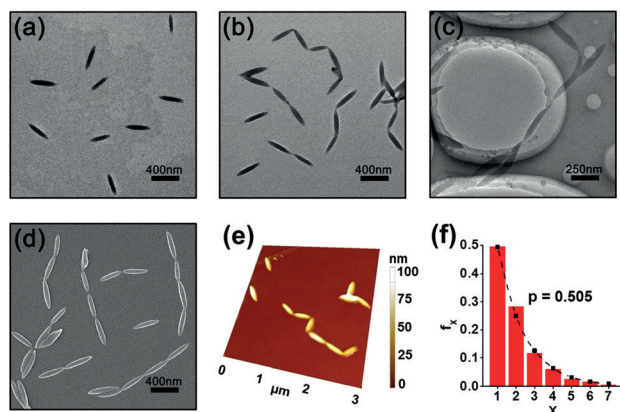

Figure 1. a) TEM image of subunits self-assembled from PBLG-*g*-PEG copolymers. b) TEM, c) cryo-TEM, d) SEM, and e) AFM images of nanowire aggregates self-assembled from subunits. f) Number fraction (f_X) of the nanowires as a function of the degree of polymerization (X). The dashed line is the theoretical number fraction (f_X) of the nanowires with X ($f_X = (1-p)p^{X-1}$).

revealed the shapes of the long micelles in three dimensions, and the height profiles (Supporting Information, Figure S2) indicated that the heights of the subunit body and connecting points were approximately 60 nm and 30 nm, respectively, thus confirming that the subunits were linked together.

Electron microscopy images also revealed that the length of the nanowires (associated with the number of repeat subunits) exhibited polydispersity. To obtain insights into the structural details of the nanowires, we calculated the number fraction f_X of the nanowires with degree of polymerization (X).[7,11] This value was obtained by collecting SEM images with more than 400 micelles and then analyzing the images using Image-Pro Plus software (Supporting Information, Section 2). Here, the degree of polymerization is defined as the number of spindles in a nanowire. As shown in Figure 1 f, f_X exhibited an exponential decay, and the number fraction of unreacted spindles (X = 1) was approximately 0.495. Therefore, the probability of finding an unreacted spindle was $1-p = 0.495$ (note that p, the extent of polymerization in step polymerization, is the fraction of spindles joining in the polymerization). It was found that the f_X data could be fitted with the relationship $f_X = (1-p)p^{X-1}$ (dashed line), which is a theoretical prediction of the number fraction distribution of polymers in step polymerization.[11] The good agreement between the experimental observations and theoretical predictions implied that the growth of nanowires follows the rules of step polymerization of monomers (Supporting Information, Section 4.6).

The limitations of current experimental techniques make obtaining a deep understanding of the mechanism underlying the hierarchical self-assembly difficult. To address this challenge, we performed dissipative particle dynamics (DPD) simulations to better understand the hierarchical self-assembly process. These simulations describe the complex hydrodynamic behavior of a set of soft particles through a set of forces on the particles, including the conservative, dissipative, and random forces.[12] The simulation details are presented in Section 3 of the Supporting Information. For this analysis, we constructed a coarse-grained model of the graft copolymer with a rigid backbone and flexible side chains to represent the PBLG-*g*-PEG copolymers (Figure 2 a). In the DPD method, a_{ij} is defined as the maximum repulsion between particle i and j. Higher a_{ij} values are correlated with stronger incompatibility. The modeled copolymers self-assembled into spindle-like micelles at repulsive parameters of $a_{RC} = 40$, $a_{RS} = 45$, and $a_{CS} = 25$, consistent with our experiments (Figure 2 b). The inset shows that the rigid backbones align and are oriented along the long axis in a manner similar to nematic liquid crystals. To simulate the second step of self-assembly, we varied the solvent conditions by tuning the interaction parameters to $a_{RC} = 40$, $a_{RS} = 100$, and $a_{CS} = 20$. Under these new solvent conditions, which corresponded to addition of DMF to the initial solution of subunits and dialyzing against water, the initial spindle-like subunits were found to further aggregate and form long nanowires (Figure 2 c). The observed nanowire aggregates also presented a polydisperse distribution in micelle size. Similar to the experiments, the number fraction f_X of the nanowires with degree of polymerization (X) was determined by collecting more than 400 micelles, obtained from repeated calculations.
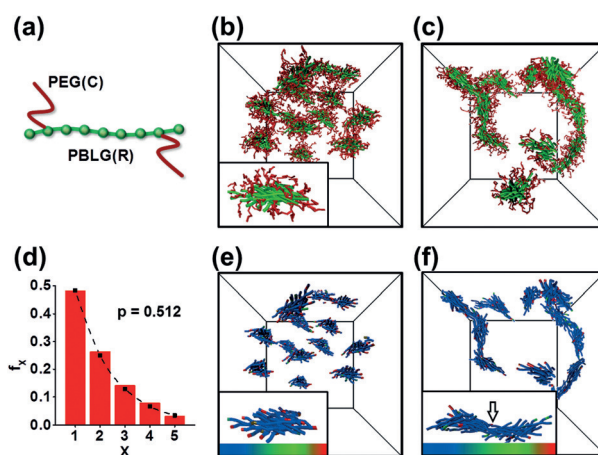

Figure 2. a) DPD model of a rod-*g*-coil graft copolymer. b,c) Simulation snapshots of spindle-like subunits ($a_{RS} = 45$ and $a_{CS} = 25$) and nanowire aggregates ($a_{RS} = 100$ and $a_{CS} = 20$), where $a_{RC} = 40$. d) Number fraction (f_X) of the nanowires with degree of polymerization (X) as a function of X. The dashed line is the theoretical values of f_X. e) Distribution of conservative energy in the subunits under new solvent conditions ($a_{RS} = 100$ and $a_{CS} = 20$), where the insert shows the energy distribution of a single subunit. The colors range from blue (low-energy region) to red (high-energy region). f) Distribution of conservative energy in nanowire aggregates at final equilibrium. The arrow in the insert indicates that the high energy disappears at the connection part of two spindle-like micelles.

As shown in Figure 2d, the f_X data could be well-fitted with the relationship $f_X = (1-p)p^{X-1}$, which corroborated our conclusion from the experimental data that the nanowires are synthesized by a step polymerization mechanism (Supporting Information, Section 4.6).

To understand the factors that drive the polymerization of the spindle-like micelles into nanowires, we calculated the conservative energies (Equation (1)):

$$\sum_{i \neq j} a_{ij}(r_i - r_j)^2 \qquad (1)$$

where a_{ij} represents the repulsive parameters, r_{ij} is the distance between beads i and j, and r_c is the cutoff radius (calculation details are provided in the Supporting Information, Section 3.2.6). The conservative energies reflect the total energy contribution to a target bead resulting from the conservative interactions with surrounding beads.[12a–c] Calculations were performed for subunits under the new solvent conditions and for nanowire aggregates at final equilibrium. The 3D energy distributions of the aggregates were obtained by coloring the backbones according to the energy values. The energy distribution in the subunits showed that the energies at the two ends of the micelles are higher than those in the body of the micelle (Figure 2e). This result indicates that the micelle ends become energetically unfavorable and consequently active (that is, they behave as reactive points) under the new solvent conditions, creating a driving force to direct the subsequent assembly of the subunits. By forming nanowires, the high-energy ends of the subunits disappear (Figure 2f). The inset of Figure 2b shows that the rigid backbones are packed parallel with respect to each other, whereas the PEG chains protrude outside to maintain stability. Because of the anisotropic nature of the spindle-like subunits, the coverage of PEG around the cores is not homogeneous. This anisotropy of the subunits enables the generation of reactive points for subsequent reaction. When DMF is added to the initial subunit solution, the polymer chains swell, resulting in more exposure of PBLG segments to the solvents at both ends. This change generates reactive points with higher energies as selective solvents (water) are added. In the second self-assembly step, PBLG segments in both micelle ends from different subunits connect with each other by physical bonding, resulting in the formation of nanowires. The increases in energy are lowered upon the formation of connected subunits. The energy analysis based on DPD simulations supports this mechanism.

The above results revealed that the reactivity of the subunit ends, which is created by adding DMF to the initial subunit solution and dialyzing against water, drives the subunits to connect together. We conducted a control experiment to verify this mechanism. As shown in our previous work,[10c] during the preparation of hybrid micelles consisting of graft and block copolymers, the block copolymers can effectively cap the ends of the cylindrical micelles to generate stable cylindrical structures with lower energy ends. Here, PBLG$_{100}$-b-PEG$_{113}$ block copolymers (the

subscripts indicate the degree of polymerization per block) were mixed with PBLG-g-PEG graft copolymers. Pre-assembled subunits with two capped ends were obtained. With these subunits, nanowire aggregates could not be obtained through a second step of self-assembly because the reactive points were not created by adding DMF (Supporting Information, Figure S3).

To deepen our understanding of the mechanism for nanowire formation, we investigated the effect of the amount of added water on the dynamic process of aggregate formation. Following the method adopted in the literature,[13] we first prepared a group of subunit solutions by adding DMF (10 mL) to the initial subunit solution. Subsequently, various amounts of water were added into each subunit solution. After equilibration, the aggregates were frozen by rapidly adding a large amount of water and then dialyzing the solution against the water. Using this method, we can observe the growth progress of the nanowires. The SEM images shown in Figures 3a–d revealed that the spindle-like subunits present limited changes with small additions of water and then gradually transformed into nanowires as the amount of water increased. Such a tendency can be clearly observed using a plot of the number fraction (f_X) of the nanowires with the degree of polymerization (X) against the value of X at each observation point (Figure 3i). The connection of the subunits is a hierarchical process of stepwise self-assembly, analogous to the step polymerization of monomers. Therefore, the nanowires can be considered products of a step polymerization of pre-assembled subunits. Correspondingly, the formation of nanowire aggregates was simulated by varying the solvent conditions from $a_{RS} = 55$ and $a_{CS} = 25$ to $a_{RS} = 100$ and $a_{CS} = 20$ in a step-by-step manner. The equilibrated structures showed that the initial spindle-like subunits connected into long nanowires step-by-step, as shown in Figures 3e–h and by the plots of f_X against X (Figure 3j). These simulation results verified the hierarchical self-assembly process. From both the experiments and simulations, we can observe some controllable characteristics of the self-assembly of subunits. For example, the length of the nanowires can be controlled by the amount of water added to
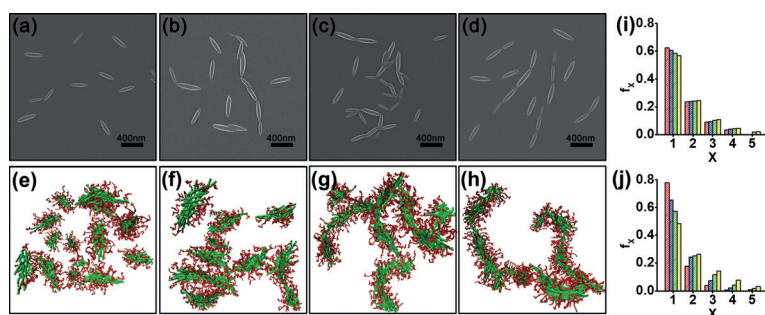

Figure 3. SEM images of the aggregates self-assembled from PBLG-g-PEG subunits with various amounts of water added to the subunit solution (scale bar, 400 nm): a) 16.7, b) 20.0, c) 23.0, and d) 26.0 wt%. Snapshots of the structures obtained by varying the solvent conditions: e) $a_{RS} = 55$, $a_{CS} = 25$; f) $a_{RS} = 60$, $a_{CS} = 24$; g) $a_{RS} = 80$, $a_{CS} = 22$; and h) $a_{RS} = 100$, $a_{CS} = 20$. The a_{RC} was fixed at 40. Plots of the number fraction (f_X) of the nanowires with degree of polymerization (X) against X at each observation point for the i) experiments (A ■; B ■; C ■; D ■) and j) simulations (E ■; F ■; G ■; H ■).

the initial subunit solution (Supporting Information, Section 4.3).

Figures 1–3 show that the emergence of reactive points is responsible for the appearance of polymerization-like self-assembly. The activity of the reactive points may affect the stepwise self-assembly behavior, similar to the manner in which functional group activity affects the step polymerization of monomers. To examine this effect, we varied the amount of DMF added to the initial subunit solution. This approach was used because the exposure of the hydrophobic PBLG segments in the subunit ends can be manipulated by the amount of DMF present. The effect of the DMF content on the activity of the reactive points can be observed in the SEM images presented in Figures 4a–d. When 1 mL of DMF was introduced to 10 mL of the initial subunit solution (volume fraction of DMF in subunit solution $\phi_{DMF} = 0.44$), several spindle-like subunits were connected in the subsequent self-assembly process. The unconnected subunits had a high number fraction, up to 0.85 (Figure 4e). As the DMF content increased, more subunits were assembled into nanowires with more repeat subunits, which was accompanied by a gradual decrease in the number fraction of unconnected subunits (Figure 4e; Supporting Information, Figure S6). The aggregate morphologies were also investigated using TEM, and the information provided by the TEM images corroborated the SEM observations (Supporting Information, Figure S7). The effect of the degree of grafting of PEG chains was subsequently studied. Tendencies in morphology evolution similar to that of PBLG-*g*-PEG copolymers were observed for both PBLG-*g*-PEG-1 and PBLG-*g*-PEG-2 copolymers with higher grafting degrees of 2.78% and 5.90%, respectively (Supporting Information, Figure S8). When the amount of DMF added to the initial subunits

solution was increased, the extent of polymerization (*p*) increased, and the nanowires lengthened under the present conditions employed (Supporting Information, Figure S9).

To characterize the average micelle size and the size distribution of the nanowire aggregates, we defined two parameters: the number-average degree of polymerization of the nanowires (X_n), which describes the number-average length of the nanowires, and the polydispersity index (PDI), which characterizes the size distribution. Details of the definitions and measurements are provided in Section 2 of the Supporting Information. X_n and PDI are shown in Figures 4f and 4g as functions of the amount of DMF added for PBLG-*g*-PEG graft copolymers with various degrees of grafting. It can be observed that X_n and PDI increase with increasing amounts of added DMF for the three graft copolymers. This result indicates that the hierarchical nanowires become longer and their size distribution becomes broader as the activity of the micelle ends increases. The influence of the degree of grafting can also be observed in Figures 4f and 4g. These data show that a higher degree of grafting leads to smaller X_n and PDI, suggesting that the nanowires become shorter and their size distribution becomes narrower as more PEG chains are grafted. This effect can be readily explained by the fact that the coverage of the subunit ends can be enhanced as more PEG chains are grafted, resulting in lower activity of the reactive points. We further examined the correlation between PDI and X_n for the data from all the graft copolymer samples. According to the theory of polymerization,[11] variations of PDI as a function of X_n satisfies $PDI = 2 - 1/X_n$, independent of monomer type, reaction activity, and reaction time. The data analyses revealed that the dependence of PDI on X_n is consistent with the theoretical predictions. This result further suggests that the polymerization of subunits follows the rules of step polymerization (Supporting Information, Section 4.6).

In addition to the degree of grafting, the effect of the PBLG backbone length was also investigated. The PBLG-*g*-PEG-3 graft copolymers, with a higher molecular weight of PBLG backbone ($M_w = 300\,000\ g\,mol^{-1}$), were chosen to conduct this experiment. The grafting degree of PEG in PBLG-*g*-PEG-3 is 3.7%. We observed that, under similar experimental conditions the subunits produced from the graft copolymer with the longer PBLG backbone were approximately 150 nm longer than the graft copolymers with the shorter backbone (Supporting Information, Figure S12). These pre-assembled subunits were observed to be capable of self-assembling into nanowire aggregates (Supporting Information, Figure S13). The obtained results also revealed that the nanowire aggregates become longer as the amount of DMF added increases and tends to be shorter when the degree of grafting is higher (Supporting Information, Figure S14). This dependence is similar to the results observed for graft copolymers with a shorter backbone. In a separate experiment, we mixed these longer pre-assembled subunits with the shorter subunits. Interestingly, nanowires with these two types of subunits connected were obtained upon addition of DMF and dialyzing against water (Supporting Information, Figure S15). This suggests that hybrid nanowires can be prepared by the copolymerization of different subunits, which
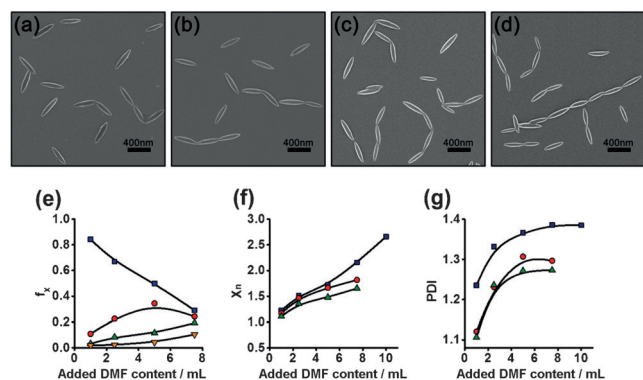

Figure 4. SEM images of nanowire aggregates self-assembled from PBLG-*g*-PEG subunits with various amounts of DMF added to 10 mL of initial subunit solution (scale bar, 400 nm): a) 1.0 ($\phi_{DMF} = 0.44$), b) 2.5 ($\phi_{DMF} = 0.50$), c) 5.0 ($\phi_{DMF} = 0.57$), and d) 7.5 mL ($\phi_{DMF} = 0.62$). e) Number fraction (f_X) of the nanowires with various degrees of polymerization (PBLG-*g*-PEG). Key: X = 1 (—■—), X = 2 (—●—), X = 3 (—▲—), X = 4 (—▼—). f) Number-average degree of polymerization (X_n) of the nanowires and g) polydispersity index (PDI) as functions of the amount of DMF added to the initial subunit solution. Degrees of grafting of PBLG-*g*-PEG, PBLG-*g*-PEG-1, and PBLG-*g*-PEG-2 were 1.23%, 2.78%, and 5.90%, respectively. Key (f) and (g): PBLG-*g*-PEG (—■—), PBLG-*g*-PEG-1 (—●—), PBLG-*g*-PEG-2 (—▲—).

further confirms the proposed mechanism for stepwise self-assembly.

In summary, a promising route for synthesizing hierarchical structures by supramolecular step polymerization is described herein. By considering the variations in free energy during the self-assembly process, we proposed a possible mechanism for the stepwise self-assembly. Figure 5 presents a schematic in which the calculation results for the free energy changes in the stepwise self-assembly process are plotted (calculation details are available in the Supporting Information, Section 3.2.6). Briefly, the PBLG-*g*-PEG graft
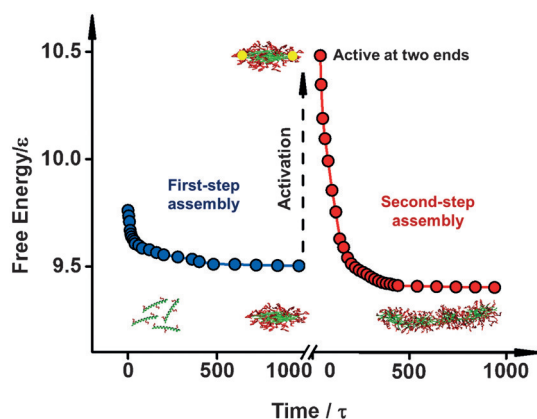

Figure 5. Variation in free energy in units of ε (energy units in DPD) as a function of simulation time for the two-step self-assembly of rod-*g*-coil graft copolymers. Upon addition of DMF to a solution of pre-assembled subunits, the subunits are activated and reactive points are generated at each end, which drives the formation of nanowire aggregates through a supramolecular step polymerization.

copolymers in THF/DMF/water mixed solvents first self-assemble into spindle-like subunits. Accordingly, the free energy decreases to an equilibrium state, as shown by the blue line (free energy was calculated for the rod-*g*-coil model). The micelles, consisting of PEG coronas and PBLG cores, are stable in the solution. Upon addition of DMF, the local structures of the spindles change in response to the change in the solvent environment. By quickly dialyzing against water, reactive points are generated at the ends of the micelles and the spindle-like micelles are activated (see the dashed arrows in Figure 5). At this point, the spindle-like micelles are far from equilibrium. The reactive points behave analogously to functional groups in a step polymerization. To reduce the high-energy defects and achieve equilibrium, the micelles self-assemble into nanowires by physical connecting PBLG segments on both subunit ends. This process effectively reduces the number of unfavorable ends and minimizes the free energy, as shown by the red line in Figure 5. The present work demonstrates a type of polymerization that occurs at the supramolecular level. The polymerization units are micelles, and the defects existing in the micelles enable the generation of reactive points for polymerization. Such polymerization could be generalized to some other polymer systems that contain rigid chains, as long as the reactive points can be produced in pre-assembled subunits (Supporting Informa-

tion, Section 4.9). Using this principle, we can design and prepare sophisticated materials with controlled structures, which may find potential applications in various fields, such as in biomedicine (Supporting Information, Section 4.10). Moreover, the present work provides a model system for studying polymerization occurring at the supramolecular level and for revealing the nature of such polymerization.

Experimental Section

PBLG was obtained by ring-opening polymerization of γ-benzyl-L-glutamate-*N*-carboxyanhydride (BLG-NCA), initiated by triethyl-amine and with 1,4-dioxane as solvent.[14] PBLG-*g*-PEG was prepared by the ester exchange reaction of PBLG with mPEG-OH.[10a, 15] At the end of the two polymerizations, the reaction mixture was precipitated into a large volume of anhydrous methanol. The product was purified twice by repeated precipitation from a chloroform solution into a large volume of anhydrous methanol and dried under vacuum. Details are shown in the Supporting Information.

Polymer assemblies were prepared in the following way. First, PBLG-*g*-PEG graft copolymers were dissolved in THF/DMF (1/1, v/v) mixed solvents by stirring at room temperature for 2 days to obtain stock solutions. Typically, deionized water (2.5 mL) was added to PBLG-*g*-PEG (10 mL) initial solution (polymer concentration is $0.67 \, \mathrm{g\,L^{-1}}$) with vigorous stirring to form subunits (initial subunit solution). Subsequently, DMF (10 mL) was pipetted into the initial subunit solution to form the subunit solution. The subunit solution was dialyzed against deionized water for 3 days to ensure that all the organic solvents were removed. The polymer concentration of the subunit solutions was fixed at $0.3 \, \mathrm{g\,L^{-1}}$ for all samples. Prior to analysis, the solutions were stabilized for at least 5 days. The nanowires can also be obtained by other methods, such as a one-step self-assembling method, indicating that a similar structure can be self-assembled by different paths (Supporting Information, Section 1.2). The morphologies were characterized by TEM (JEM-2100F, JEOL, 200 kV), SEM (S4800, Hitachi, 15 kV), Cryo-TEM (JEM-2200FS, CEVS, 200 kV, −174 °C), and AFM (XE-100, Park Systems, non-contact mode). Details are available in the Supporting Information.

DPD is a particle-based mesoscopic simulation technique for complex fluids.[12a,b] In the simulation, each bead represents a block or cluster of atoms or molecules. The time evolution of the beads obeys Newton's equation of motion. In this equation, the total force is the sum of conservative, dissipative, and random forces. The simulations were conducted in a cubic box of $30 \times 30 \times 30$ with periodic boundary conditions, and an NVT ensemble was adopted. Details regarding the simulations can be found in the Supporting Information.

[1] a) R. Lakes, *Nature* **1993**, *361*, 511–515; b) D. A. Tirrell in *Hierarchical Structures in Biology as a Guide for New Materials Technology*, National Academic Press, Washington DC, **1994**.

[2] L. Hagelskjaer, I. Sørensen, E. Randers, *Scand. J. Infect. Dis.* **1998**, *30*, 309–311.

[3] a) X. Yan, G. Liu, Z. Li, *J. Am. Chem. Soc.* **2004**, *126*, 10059–10066; b) C. Sanchez, H. Arribart, M. Madeleine, G. Guille, *Nat. Mater.* **2005**, *4*, 277–288; c) T. Gädt, N. S. Ieong, G. Cambridge, M. A. Winnik, I. Manners, *Nat. Mater.* **2009**, *8*, 144–150; d) F. He, T. Gädt, I. Manners, M. A. Winnik, *J. Am. Chem. Soc.* **2011**, *133*, 9095–9103; e) A. H. Gröschel, A. Walther, T. I. Löbling, F. H. Schacher, H. Schmalz, A. H. E. Müller, *Nature* **2013**, *503*, 247–251; f) A. H. Gröschel, F. H. Schacher, H. Schmalz, O. V. Borisov, E. B. Zhulina, A. Walther, A. H. E. Müller, *Nat. Commun.* **2012**, *3*, 710.

[4] a) S. Jain, F. S. Bates, *Science* **2003**, *300*, 460–464; b) D. E. Discher, A. Eisenberg, *Science* **2002**, *297*, 967–973; c) J. Rodríguez-Hernández, S. Lecommandoux, *J. Am. Chem. Soc.* **2005**, *127*, 2026–2027.

[5] a) X. Wang, G. Guerin, H. Wang, Y. Wang, I. Manners, M. A. Winnik, *Science* **2007**, *317*, 644–647; b) Q. Chen, H. Zhao, T. Ming, J. Wang, C. Wu, *J. Am. Chem. Soc.* **2009**, *131*, 16650–16651; c) L. Zhang, C. Bartels, Y. Yu, H. Shen, A. Eisenberg, *Phys. Rev. Lett.* **1997**, *79*, 5034–5037; d) C. Cai, Y. Li, J. Lin, L. Wang, S. Lin, X. Wang, T. Jiang, *Angew. Chem. Int. Ed.* **2013**, *52*, 7732–7736; *Angew. Chem.* **2013**, *125*, 7886–7890.

[6] a) A. Walther, C. Barner-Kowollik, A. H. E. Müller, *Langmuir* **2010**, *26*, 12237–12246; b) S. A. Jenekhe, X. L. Chen, *Science* **1999**, *283*, 372–375; c) H. Cui, Z. Chen, S. Zhong, K. L. Wooley, D. J. Pochan, *Science* **2007**, *317*, 647–650; d) A. Hanisch, A. H. Gröschel, M. Förtsch, M. Drechsler, H. Jinnai, T. M. Ruhland, F. H. Schacher, A. H. E. Müller, *ACS Nano* **2013**, *7*, 4030–4041; e) H. Qiu, G. Russo, P. A. Rupar, L. Chabanne, M. A. Winnik, I. Manners, *Angew. Chem. Int. Ed.* **2012**, *51*, 11882–11885; *Angew. Chem.* **2012**, *124*, 12052–12055; f) B. Fang, A. Walther, A. Wolf, Y. Xu, J. Yuan, A. H. E. Müller, *Angew. Chem. Int. Ed.* **2009**, *48*, 2877–2880; *Angew. Chem.* **2009**, *121*, 2921–2924; g) J. Zhu, S. Zhang, F. Zhang, K. L. Wooley, D. J. Pochan, *Adv. Funct. Mater.* **2013**, *23*, 1767–1773.

[7] a) K. Liu, Z. Nie, N. Zhao, W. Li, M. Rubinstein, E. Kumacheva, *Science* **2010**, *329*, 197–200; b) K. Liu, A. Lukach, K. Sugikawa, S. Chung, J. Vickery, H. Therien-Aubin, B. Yang, M. Rubinstein, E. Kumacheva, *Angew. Chem. Int. Ed.* **2014**, *53*, 2648–2653; *Angew. Chem.* **2014**, *126*, 2686–2691.

[8] H. Cui, Z. Chen, S. Zhong, K. L. Wooley, D. J. Pochan, *Science* **2007**, *317*, 647–650.

[9] a) J. Ding, G. Liu, *Macromolecules* **1999**, *32*, 8413–8420; b) J. Dupont, G. Liu, K. Niihara, R. Kimoto, H. Jinnai, *Angew. Chem. Int. Ed.* **2009**, *48*, 6144–6147; *Angew. Chem.* **2009**, *121*, 6260–6263; c) X. Yan, G. Liu, J. Hu, *Macromolecules* **2006**, *39*, 1906–1912; d) Z. Li, J. Ma, N. S. Lee, K. L. Wooley, *J. Am. Chem. Soc.* **2011**, *133*, 1228–1231; e) J. A. A. W. Elemans, A. E. Rowan, R. J. M. Nolte, *J. Mater. Chem.* **2003**, *13*, 2661–2670.

[10] a) C. Cai, J. Lin, T. Chen, X. Tian, *Langmuir* **2010**, *26*, 2791–2797; b) C. Cai, L. Wang, J. Lin, *Chem. Commun.* **2011**, *47*, 11189–11203; c) Z. Zhuang, X. Zhu, C. Cai, J. Lin, L. Wang, *J. Phys. Chem. B* **2012**, *116*, 10125–10134; d) C. Cai, J. Lin, Z. Zhuang, W. Zhu, *Adv. Polym. Sci.* **2013**, *259*, 159–199.

[11] G. Odian, *Principles of Polymerization*, 4th ed., Wiley, New York, **2004**.

[12] a) P. J. Hoogerbrugge, J. M. V. A. Koelman, *Europhys. Lett.* **1992**, *19*, 155–160; b) J. M. V. A. Koelman, P. J. Hoogerbrugge, *Europhys. Lett.* **1993**, *21*, 363–368; c) T. Jiang, L. Wang, S. Lin, J. Lin, Y. Li, *Langmuir* **2011**, *27*, 6440–6448; d) Y. Li, T. Jiang, S. Lin, J. Lin, C. Cai, X. Zhu, *Sci. Rep.* **2015**, *5*, 10137.

[13] a) L. Zhang, A. Eisenberg, *Macromolecules* **1999**, *32*, 2239–2249; b) J. Zhu, Y. Liao, W. Jiang, *Langmuir* **2004**, *20*, 3809–3812; c) C. Cai, J. Lin, X. Zhu, S. Gong, X.-S. Wang, L. Wang, *Macromolecules* **2016**, *49*, 15–22.

[14] a) E. R. Blout, R. H. Karlson, *J. Am. Chem. Soc.* **1956**, *78*, 941–946; b) C. Cai, W. Zhu, T. Chen, J. Lin, X. Tian, *J. Polym. Sci. Part A* **2009**, *47*, 5967–5978.

[15] K. Inomata, N. Ohara, H. Shimizu, T. Nose, *Polymer* **1998**, *39*, 3379–3386.